International Journal of Pharmaceutics 646 (2023) 123431

Contents lists available at ScienceDirect

International Journal of Pharmaceutics

journal homepage: www.elsevier.com/locate/ijpharm

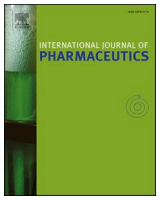

Liquid crystalline nanogel targets skin cancer via low-frequency ultrasound treatment

Tatiana Aparecida Pereira [a], Danielle Nishida Ramos [a], Lays Martin Sobral [a], Yugo Araújo Martins [a], Raquel Petrilli [a,b], Márcia de Abreu Carvalho Fantini [c], Andréia Machado Leopoldino [a], Renata Fonseca Vianna Lopez [a,*]

[a] School of Pharmaceutical Sciences of Ribeirao Preto, University of Sao Paulo, Av. Cafe s/n, 14040-903 Ribeirao Preto, SP, Brazil
[b] Institute of Health Sciences, University of International Integration of the Afro-Brazilian Lusophony, Redenção, Brazil
[c] Institute of Physics, University of São Paulo, Rua do Matão 1371, 05508-090 São Paulo-SP, Brazil

ARTICLE INFO

Keywords:
Low frequency ultrasound
Doxorubicin
Skin cancer therapy
Sonophoresis
Topical treatment

ABSTRACT

The potential of low-frequency ultrasound (LFU) combined with nanotechnology-based formulations in improving skin tumors topical treatment was investigated. The impact of solid lipid nanoparticles (SLN) and hydrophilic nanogels as coupling media on LFU-induced skin localized transport regions (LTR) and the penetration of doxorubicin (DOX) in LFU-pretreated skin was evaluated. SLN were prepared by the microemulsion technique and liquid crystalline nanogels using Poloxamer. In vitro, the skin was pretreated with LFU until skin resistivity of ~1 KΩ.cm^2 using the various coupling media followed by evaluation of DOX penetration from DOX-nanogel and SLN-DOX in skin layers. Squamous cell carcinoma (SCC) induced in mice was LFU-treated using the nanogel with the LFU tip placed 5 mm or 10 mm from the tumor surface, followed by DOX-nanogel application. LFU with nanogel coupling achieved larger LTR areas than LFU with SLN coupling. In LFU-pretreated skin, DOX-nanogel significantly improved drug penetration to the viable epidermis, while SLN-DOX hindered drug transport through LTR. *In vivo*, LFU-nanogel pretreatment with the 10 mm tip distance induced significant tumor inhibition and reduced tumor cell numbers and necrosis. These findings suggest the importance of optimizing nanoparticle-based formulations and LFU parameters for the clinical application of LFU technology in skin tumor treatment.

1. Introduction

Skin cancer is the most frequent cancer type, with more than one million diagnoses yearly (D'Orazio et al., 2013). It is categorized into melanoma and non-melanoma skin cancer based on the cell type. Non-melanoma skin cancer includes basal and squamous cell carcinoma (SCC), with the latter being more aggressive. Topical treatment is a promising strategy for skin cancer management, alone or in combination with conventional treatments. This approach offers simple administration, easy accessibility, non-invasiveness, limited adverse effects at the application site, low risk of functional impairment, and improved aesthetic outcomes (Petrilli et al., 2018).

However, the stratum corneum (SC), the outermost layer of the skin, poses a major obstacle to topical treatment of skin tumors due to its impermeable "brick and mortar" structure (Nemes and Steinert, 1999; Schoellhammer et al., 2014). To enhance drug delivery to the skin, researchers have explored lipid nanoparticles for many years (Krishnan and Mitragotri, 2020). Among them, solid lipid nanoparticles (SLN), composed of surfactants and solid lipids at room and body temperature, are particularly attractive due to their ability to increase drug stability and provide controlled release. These nanoparticles are non-toxic, biocompatible, and biodegradable (Mehnert and Mader, 2001).

In addition to nanotechnology-based formulations, other technologies, like low-frequency ultrasound (LFU), have been investigated to improve drug penetration into the skin. By applying LFU in the frequency range of 20 to 60 kHz, the skin's barrier, specifically the SC, can be overcome by creating localized transport regions (LTR) that are approximately 80% more permeable than non-LTR regions (Kushner

* Corresponding author at: School of Pharmaceutical Sciences of Ribeirão Preto, University of São Paulo, Av. do Café sn, CEP 14040-903, Ribeirao Preto-SP, Brazil.
E-mail addresses: tatiana.pereira@uniube.br (T.A. Pereira), ramos.dnr@gmail.com (D.N. Ramos), lays.martinsobral@cuanschutz.edu (L.M. Sobral), yugomartins@usp.br (Y.A. Martins), petrilliraquel@unilab.edu.br (R. Petrilli), mfantini@if.usp.br (M.A.C. Fantini), andreiaml@usp.br (A.M. Leopoldino), rvianna@fcfrp.usp.br (R.F.V. Lopez).

https://doi.org/10.1016/j.ijpharm.2023.123431
Received 9 May 2023; Received in revised form 5 September 2023; Accepted 19 September 2023
Available online 20 September 2023

et al., 2004). Another advantage of LFU is its ability to permeabilize tumor cells, facilitating intracellular drug uptake (Shibaguchi et al., 2011; Zolochevska et al., 2011).

Combining LFU with SLN can be advantageous in targeting anticancer drugs to specific skin layers where tumors are located, thus providing a high drug concentration to the tumor cells. However, the influence of lipid nanoparticles on LTR formation remains unknown, especially concerning the hydrophilic character of LTR (Petrilli and Lopez, 2018) and their lifetime. As skin permeability is closely related to LTR, investigating nanoparticles' influence on LTR distribution and drug permeability through nanoparticle-modified LTR is essential. This search is crucial for further developing nanotechnology-based formulations to treat skin tumors combined with LFU.

Furthermore, topical treatment uses semi-solid dosage forms to keep the formulation at the application site. Nanocarrier dispersions are often thickened with the addition of polymers (Patel et al., 2020; Shivam et al., 2020), with poloxamers being a notable choice.

Poloxamers are synthetic triblock copolymers composed of poly (ethylene oxide)–poly (propylene oxide)–poly (ethylene oxide), widely used as gel-forming agents that act *in situ* at body temperature. These copolymers self-organize into micellar aggregates that behave as sols, flowing freely at low temperatures. However, at high temperatures, dehydration of the hydrophilic chains and entanglement with hydrophobic ones increase mechanical resistance, resulting in viscous gels. In this form, the micelles remain compacted, resembling crystallized spheres (Mortensen and Brown, 1993), and are called nanogels (Cho et al., 2019; Jeswani et al., 2021). Beyond the nanogels' role as topical controlled drug delivery systems, they have demonstrated skin penetration-enhancing properties (Shah et al., 2012).

Formulations that combine nanocarriers like SLN with polymeric dispersions, such as poloxamer nanogels, are already complex delivery systems. When combined with ultrasonic stimulation, they can undergo modifications that ultimately affect LTR formation, nanoparticle interaction with the skin, and drug interactions with the nanocarrier and the skin. For instance, as hydrophilic nanocarriers, nanogels may influence the formation of skin-LTR induced by LFU and modulate drug penetration through LTR in a manner distinct from lipophilic SLN.

In this context, the present study aims to evaluate the impact of SLN, nanogel, and their association (SLN-nanogel) on LTR induced by LFU and on the cutaneous penetration of a model chemotherapy drug, doxorubicin in LFU-pretreated skin. *In vivo* studies were conducted using a xenograft animal model to evaluate the potential applicability of the LFU-nanoparticle association in the SCC treatment and the impact of the experimental protocol on treatment outcomes.

2. Materials and methods

2.1. Materials

Doxorubicin hydrochloride (DOX) was sourced from Zodiac (Sao Paulo, SP, Brazil). Stearic acid and Allura red were purchased from Sigma Aldrich Co. (St. Louis, MO, USA). Monoolein (Myverol®18-92 K) was obtained from Kerry (Campinas, SP, Brazil), while hexadecyltrimethylammonium bromide (CTAB) was acquired from Vetec (Rio de Janeiro, RJ, Brazil). Poloxamer 407® (Poloxamer) was supplied by Embrafarma (Sao Paulo, SP, Brazil). Additional chemicals and reagents included HEPES (4-(2-hydroxyethyl)-1-piperazineethanesulfonic acid), isopropanol, and acetonitrile from J. T. Baker (Phillipsburg, New Jersey, USA), and phosphate buffer solution (PBS) salts (monobasic potassium phosphate, dibasic sodium phosphate, and NaCl) from Synth (São Paulo, SP, Brazil). Ag/AgCl electrodes were sourced from In Vivo Metrics (Healdsburg, CA, USA). For cell culture, fetal bovine serum (FBS), trypsin, and Dulbecco's modified Eagle's medium (DMEM) were obtained from Gibco (Grand Island, NY, USA) as well as the Antibiotic/Antimycotic Solution containing 10,000 units/mL penicillin, 10 mg/mL streptomycin, and 25 μg/mL amphotericin B. Tissue Tek (OCT Compound) was purchased from Sakura (Torrance, CA, USA). The A431 cell line (ATCC® CRL1555™) was acquired from the American Type Culture Collection (ATCC) and cultivated following the supplier's instructions.

2.2. SLN preparation

SLN were prepared by the microemulsion technique, as previously described (Huber et al., 2015). Briefly, an aqueous solution containing CTAB (140 mg) was transferred to a melted lipid phase (800 mg of stearic acid and 260 mg of monoolein) under magnetic stirring (300 rpm) until a thermodynamically stable microemulsion was formed. The SLN dispersion was obtained by cooling the microemulsion in cold water at a 1:20 ratio (microemulsion/cold water) under vigorous stirring at 20,000 rpm (IKA T-25 Ultra-turrax, Baden-Württemberg, Germany) for 10 min. SLN-DOX was obtained by adding 32 mg of DOX (4% of the lipid phase) to the melted lipid phase before the microemulsion formation. SLN aqueous dispersions were processed using high-pressure homogenization (Emulsi Flex C3, Mannheim, Germany) at 500 bars for 10 min.

2.3. SLN characterization

2.3.1. Physicochemical characterization

Nanoparticles were characterized by particle size, zeta potential, and encapsulation efficiency. The mean particle size and polydispersity (PdI) were measured by photon correlation spectroscopy (PCS) using a Malvern Zetasizer ZS 90 with a fixed angle of 90° (Malvern Instruments, Worcestershire, England). Zeta potential was determined by electrophoretic mobility using the same instrument. Samples were diluted in purified water (1:10) at 25 °C. All analyses were carried out in triplicate.

DOX encapsulation efficiency (EE) was calculated according to Equation I. The total amount of DOX (Qt) was obtained after solubilizing the SLN-DOX in ethanol (1:7). Its quantification by UV–Vis at 480 nm was conducted using a linear calibration curve prepared in ethanol over the concentration range of 10 to 60 $\mu g.mL^{-1}$. Free DOX (Qf) was obtained using an ultrafiltration unit containing a membrane concentrator (Amicon®, MWCO 100 K, Millipore Corporation, Massachusetts, USA) by the ultracentrifugation of 1 mL SLN-DOX for 40 min at 1605 g at 25 °C (Heraeus Megafuge 16 R Thermo Scientific, Massachusetts, USA). Qf was quantified using an aqueous calibration curve in the linear range of 10 to 60 $\mu g.mL^{-1}$ ($y = 0.0146x + 0.0657$, $r^2 = 0.9918$) (Huber et al., 2015).

$$EE\,(\%) = \frac{Qt - Qf}{Qt} x100 \quad (1)$$

Where: *Qt* is the total amount of DOX added to prepare the formulation, and *Qf* is the amount of free DOX.

2.3.2. Morphological characterization

The morphology of SLN-DOX was examined using an atomic force microscope (AFM). To prepare the samples, freshly cleaved mica sheets (Muscovite Mica Substrates, SPI Supplies®) were immersed in the aqueous dispersion of SLN-DOX. Subsequently, the samples were left to dry at room temperature overnight. AFM imaging was performed by scanning the surface of the mica using a cantilever with a 1.4 Hz resonance frequency, covering an area of 2 μm × 2 μm at room temperature. Both phase and topology images were captured and analyzed to determine the size and morphology of SLN-DOX.

2.4. Nanogel containing SLN, SLN-DOX, and free DOX preparation

Poloxamer (40% w/w) was solubilized in purified water (5 °C) under constant stirring until the complete dispersion of the polymer (Gratieri et al., 2010) to obtain the nanogel (Shah et al., 2020). SLN or SLN-DOX (without further purification, that is, containing free and encapsulated

DOX) was added to the poloxamer dispersion at a 1:1 v/v ratio under constant stirring, resulting in a 20% Poloxamer nanogel containing SLN (SLN-nanogel) or SLN-DOX (SLN-DOX nanogel). The theoretical concentration of the SLN components in the final nanogel was 19 $mg.mL^{-1}$ of stearic acid, 3.3 $mg.mL^{-1}$ of CTAB, 6.2 $mg.mL^{-1}$ of monoolein, and 0.4 $mg.mL^{-1}$ of DOX when SLN-DOX was used.

The nanogel containing DOX (DOX-nanogel) was obtained by adding 0.4 $mg.mL^{-1}$ DOX directly to the nanogel at 20% Poloxamer under an ice bath and constant stirring, resulting in the same concentration of DOX as the nanogel containing the SLN-DOX.

The formulations were refrigerated (4 °C) for 24 h for stabilization before the characterization.

2.5. Characterization of nanogel formulations

2.5.1. Polarized light microscopy

The formation of liquid crystalline phases in the SLN, nanogel, and the SLN-nanogel were analyzed under an Axioplan 2 optical microscope (Carl Zeiss AG, Germany) equipped with a polarizing filter and coupled to an Axio-Cam HRc digital camera (Carl Zeiss AG, Germany) with a v. ideo system and automatic image acquisition. The analyses were performed using 10 μL of the samples at 25 °C, 24 h after formulation preparation.

2.5.2. Small-angle synchrotron radiation x-ray scattering (SAXS)

The liquid crystalline phases in the SLN dispersions and nanogels (containing or not SLN) were characterized by SAXS. The selected wavelength was 0.1608 nm, and the diffraction image was integrated into the scattering vector q ($q = 4\pi \sin \theta/\lambda$). The samples were placed into glass capillaries with an internal diameter of 1.5 mm. The measurements were conducted using a bidirectional detector, with an exposure time of 600 s at 25 °C. The data were corrected for detector homogeneity, incident beam intensity, sample absorption, and dark noise subtraction. The liquid crystalline structures of samples were determined after calculating the interplanar distances and the lattice parameters (Petrilli et al., 2016).

2.5.3. Rheology analysis

The rheological properties of the nanogels containing or not the SLN were investigated under continuous shear stress. Its behavior was evaluated by plotting the shear rate [1 / s] as a function of the shear stress [Pa]. The rheology analyses used a cone and plate rheometer (Brookfield R/S Plus PTR-I) coupled to a P50-1 Cone. Continuous flow measurements were performed by increasing the rotation speed from 0 to 300 rpm for 30 s, followed by the same decrease for 30 s. Data acquisition was performed every second, totaling 30 measurements. The software RHEOCALC V1.01 (Brookfield, Stoughton, MA, USA) was used to evaluate different rheological models fitting to the data and to characterize the behavior of the samples. The model of Herschel-Bulkley was used to calculate the apparent viscosity and yield stress (Souza et al., 2017).

2.5.4. Surface tension determination

The surface tension (γ) of the SLN and the SLN-nanogel was determined with a tensiometer (Fisher Scientific, model 20) based on the Du Nouy method (Ebnesajjad, 2006), using a rigid platinum ring (Equation II).

$$F = 2\,(R1 + R2)\gamma \tag{2}$$

Where F is the displacement force, and R1 and R2 are the inner and outer radii of the ring.

All measurements were performed at room temperature (25 ± 2 °C). The surface tension of the purified water at this temperature was 73.3 $mN.m^{-1}$.

2.6. In vitro skin penetration studies

2.6.1. Skin pretreatment with LFU

Porcine ear skin was carefully dissected and dermatomed to achieve a thickness of 700 μm. Subsequently, the skin was placed over a nylon membrane (150 μm opening nylon mesh; Sefar Lab Pak, Depew New York, USA) to provide mechanical support and tightly fitted into a custom-made Franz diffusion cell. The diffusion area of the cell was 1.13 cm^2, and the receptor compartment had a volume of 13 cm^3.

Before initiating the LFU experiments, the donor and receptor chambers were filled with PBS at pH 7.4, and skin resistivity was assessed following established protocols (Pereira et al., 2017; Tang et al., 2001). The procedure involved inserting Ag/AgCl electrodes into both donor and receptor compartments. An alternating current (100 mV-RMS and 10 Hz) was applied using a signal generator (model 33210A, Agilent), and the current crossing the skin was measured using the electrode in the donor compartment connected to a multimeter. Skin resistance was determined using Ohm's law, and the resistivity was calculated by multiplying the resistance value with the available skin permeation area (1.13 cm2). Per previous studies, the minimum skin resistivity was set at 50 $K\Omega.cm^2$ (Polat et al., 2011a).

LFU skin pretreatment was performed by adding 1 mL of the coupling medium to the skin in the donor compartment and filling the receptor compartment with PBS. A 20 kHz LFU (Sonics & Materials, VCX 500, Newtown, CT, USA) with a spatial average temporal intensity (I_{sata}) of 9.6 ± 0.5 W/cm^2 and a 50% duty cycle (5 s on, 5 s off) was employed. The transducer tip was positioned at 5 mm from the skin surface in the coupling medium. The skin was treated with LFU until its electrical resistivity, measured every 1 min of treatment, reached 0.7 ± 0.2 $K\Omega.cm^2$ (Martins et al., 2020; Pereira et al., 2017). The coupling medium was changed every minute to prevent thermal effects, and the skin resistivity was measured in PBS after each coupling medium exchange (Pereira et al., 2017).

Following LFU pretreatment, the skin was thoroughly washed with PBS to remove any excess coupling medium from its surface. The receptor solution was then replaced with HEPES buffer at pH 7.4. The donor compartment was filled either with 1 mL of Allura red solution for staining the LTRs and determining the skin area occupied by them (section 2.6.2) or with the desired DOX-nanoformulation for the subsequent drug skin permeation studies through the pretreated skin (section 2.6.3).

2.6.2. Evaluation of LFU-induced skin LTR using nanogel, SLN, and SLN-nanogel as coupling media

The influence of the nanogel, SLN, and SLN-nanogel on LFU-induced skin LTR formation was evaluated using these dispersions as coupling media (n = 10). LFU was applied to the skin until a resistivity of 0.7 ± 0.2 $K\Omega.cm^2$ was reached, as previously described. After complete permeabilization of the skin with LFU, the coupling medium was washed off, and 1 mL of Allura red solution (0.025% w/v in PBS) was applied to the donor compartment for 1 h for staining of the LTR formed in the skin.

Images of the skin surface were acquired using a digital camera (Panasonic Lumix, 16.0 megapixels, auto macro function) positioned 20 cm above the skin. According to the published standardized protocol, the images were processed using Adobe Photoshop CS3 (Schoellhammer et al., 2012). In summary, firstly, the blue channel of the image was isolated to enhance the contrast and facilitate the measurement of the red portion of the skin. Subsequently, the image threshold was carefully adjusted to accurately capture only the skin area that was marked by the dye. Once an appropriate threshold was determined, the same threshold level was applied consistently to all the images. The area of the adjusted image was then quantified using Image J (National Institute of Health, Bethesda, MD). The "particle analysis" option with standard size and circularity settings was employed for this quantification process (Schoellhammer et al., 2012).

2.6.3. Evaluation of DOX penetration in LFU-pretreated skin

After skin LFU pretreatment with each coupling medium (nanogel, SLN, and SLN-nanogel) as described above, DOX-nanogel or SLN-DOX nanogel (n = 6) was applied to the donor compartment, corresponding to 400 μg DOX. The receptor chamber was filled with 13 mL of HEPES buffer pH 7.4, which was kept at room temperature (25 ± 2 °C) and magnetic stirring at 300 rpm. One milliliter of receptor media was collected at specific time points for 26 h and replaced with fresh media. High-performance liquid chromatography (HPLC) quantified DOX in the receptor solution (Section 2.8).

DOX skin retention was evaluated at the end of the experiment by carefully removing the skin from the Franz diffusion cells. DOX was extracted from the various skin layers using a validated method as previously described (Herai et al., 2007; Taveira et al., 2009; Taveira et al., 2012; Pereira et al., 2017). Briefly, the SC was separated from the skin using 15 adhesive tapes (Scotch Book Tape no. 845, 3 M, St. Paul, MN). All tapes containing the SC were immersed in 5 mL of methanol and vortex-mixed for 3 min. The methanol phase was filtered through a 0.45 μm filter preliminary HPLC analysis. The remaining portion of the skin (i.e., the skin without SC, named viable epidermis) was cut into small pieces and homogenized using a tissue homogenizer for 1 min at 3000 rpm (IKA T-25 Ultra-turrax, Baden-Württemberg, Germany), and bath-sonicated (Quimis, Q335 model, 40 kHz, São Paulo, Brazil) for 30 min in 5 mL of methanol. Finally, the resulting skin homogenate was centrifuged for 10 min, and the supernatant was filtered for DOX quantification by HPLC (Section 2.8).

2.7. Preliminary assessment of LFU pretreatment effects on SCC in vivo: Small cohort analysis

In vivo, preliminary studies were undertaken to explore the potential of the LFU-nanoparticle association in SCC treatment. The nanogel served as the coupling medium for LFU pretreatment (LFU-nanogel), and DOX-nanogel was employed as the nanocarrier for DOX in LFU-permeabilized skin. The overarching aim was to evaluate potential effects and emergent patterns linked to LFU parameters for skin tumor therapy. To conduct this investigation, a xenograft animal model was implemented in mice by grafting human SCC isolated from a skin tumor (A431) on the back of the animals.

The *in vivo* studies adhered to the guidelines set forth by the National Institutes of Health (NIH) for the Care and Use of Laboratory Animals (as approved by the Committee of Research and Ethics of the University of São Paulo, School of Pharmaceutical Sciences of Ribeirão Preto - FCFRP-USP, under authorization number n° 11.1.727.53.1).

Twenty-nine female BALB/c nude mice, aged between 12 and 16 weeks and weighing 18 to 20 g, were procured from the animal facility center at FCFRP-USP. The mice were handled under aseptic conditions in a laminar flow environment. Before inducing tumors, A431 SCC cells were cultured in DMEM containing 10% heat-inactivated FBS and 1% (v/v) Antibiotic/Antimycotic Solution at 37 °C in a 5% CO_2 atmosphere.

Tumor induction was executed by subcutaneously injecting $2x10^6$ A431 cells per animal into the dorsal region of the mice. The commencement of LFU-nanogel pretreatment and DOX-nanogel treatments occurred 10 days post-tumor induction, coinciding with tumors reaching an approximate volume of 150 mm^3.

Given the preliminary nature of the study, which aimed to optimize experimental conditions for future larger-scale *in vivo* investigations, determining the number of animals per group was guided by G*power 3.1.7.9 software (Hickey et al., 2018; Kang, 2021). The software analysis considered a significance level of 0.05, a test power of 0.8, and a substantial effect size of 0.85. Four treatment groups were established: ultrasound at distances of 5 mm and 10 mm from the skin, a negative control (no treatment), and a passive control (DOX-nanogel passively administered). The total number of animals required was established at 20, with 5 animals allocated to each of the 4 groups. Additionally, for the standardization of the LFU pretreatment time, an additional 9 animals were employed, as detailed in the subsequent subsection.

2.7.1. Standardization of in vivo LFU pretreatment application time

A preliminary pilot study was conducted on healthy animals to establish a consistent timeframe for *in vivo* LFU pretreatment (n = 6). The objective was to achieve skin resistivity levels similar to those in the corresponding *in vitro* investigations. To achieve this, using silicone grease, a glass chamber with an opening area of 2.54 cm^2 was affixed to the dorsal skin of healthy mice (animals without tumors). Nanogel was introduced into the chamber as the coupling medium, and the ultrasound probe was immersed in the nanogel, positioned 5 mm from the skin surface. Initially, the LFU parameters in the first three animals mirrored those employed in the *in vitro* experiment: 20 kHz LFU at 9.6 ± 0.5 W/cm^2, with a 5-second on/off cycle during 1 min of LFU application.

An electrode was inserted into the glass chamber after the 1 min LFU application, replacing the coupling medium with PBS pH 7.4 to evaluate the skin resistivity. A reference electrode was affixed to the mouse's tail using an IOMED® electrode patch (Utah, USA). An alternating current of 100 mV and 10 Hz was applied using a 20 MHz function/arbitrary waveform generator (Agilent, 33220A model, Santa Clara, USA), as previously described in the *in vitro* experiment (section 2.6.1). The resulting electric current passing through the skin was measured using a multimeter (Minipa, ET1450 model, São Paulo, Brazil) and subsequently used to calculate skin resistance based on Ohm's law.

The area of skin subjected to LFU treatment was excised from the animals after the 1 min LFU treatment to verify whether the electric resistivity determined in this manner corresponded to that defined *in vitro*. This dissected skin section was placed within a vertical diffusion cell, and resistivity was re-measured following established protocols (Tang et al., 2001), as outlined in section 2.6.1.

In response to the initial data on skin electrical resistivity, three additional healthy animals were utilized to monitor the electric current across the skin during each 5-second cycle of LFU application. This observation continued until the electrical resistivity approached the threshold of 1 kΩ.cm^2.

A similar procedure was initially applied to tumor-bearing mice (n = 3). However, despite visible skin lesions, the predetermined resistivity threshold of 1 kΩ.cm^2 was not achieved even after 5 complete 5-second application cycles. Consequently, a decision was made to refine the LFU application time for the tumor treatment to 2 complete 5-second cycles (5 s ON: 5 s OFF), as described in the next section.

2.7.2. Assessing how LFU tip-to-tumor distance affects SCC inhibition by DOX-nanogel post LFU-nanogel pretreatment

A preliminary evaluation was carried out to investigate the influence of DOX-nanogel on tumor growth inhibition following LFU-nanogel pretreatment, with the LFU tip positioned at two different distances from the tumor surface (5 and 10 mm). This assessment aimed to offer a comprehensive perspective on the impact of LFU experimental protocol in treating SCC.

The animal groups were allocated randomly into four distinct categories, each consisting of five animals: 1) Control group, receiving no treatment (Control); 2) DOX-nanogel administration without LFU pretreatment (Passive Treatment); 3) DOX-nanogel administration after LFU-nanogel pretreatment with the LFU tip positioned 5 mm from the tumor surface (5 mm-LFU); and 4) DOX-nanogel administration after LFU-nanogel pretreatment with the LFU tip placed 10 mm from the tumor surface (10 mm-LFU).

Before LFU application, the animals were anesthetized using a mixture of ketamine 10% / xylazine 20 mg/mL / physiological solution (1:2:7, v/v/v). An open plastic chamber featuring an opening area of 2.54 cm^2 was placed over the tumor site, housing the nanogel as the coupling medium. Employing a 20 kHz LFU device with an I_{sata} of 9.6 ± 0.5 W/cm^2 and a 50% duty cycle (5 s on, 5 s off), the LFU tip was submerged within the coupling nanogel. LFU was applied to the tumors

for 2 consecutive 5-second cycles (5 s on/5 s off), resulting in a cumulative application time of 20 s, with 10 s of LFU activation. During this process, the nanogel was replaced after the first 5-second cycle to mitigate potential thermal effects.

For the 5 mm-LFU and 10 mm-LFU groups, LFU pretreatment was applied every 3 days over 15 days, resulting in 5 LFU applications. Simultaneously, about 6 mg/Kg DOX-nanogel (300 μL of the formulation containing 120 μg of DOX) was administered daily over 15 days across both LFU-treated and non-LFU-treated (passive) groups, amounting to a cumulative total of 15 passive applications. After the 15-day treatment regimen, the animals were observed for an additional 6 days before being humanely sacrificed on the 21st day, enabling histological examination of the tumors.

Tumor dimensions were calculated employing Equation III (Molavi et al., 2008).

$$V\left(mm^3\right) = 0.5\,x\,Dxd^2 \quad (3)$$

Where V is the tumor volume, and D and d are the largest and smallest diameter.

The end time of the experiment was on the 21st day when the animals were euthanized. Tumors were then excised, fixed using 10% neutral buffered formalin, and processed for histological analysis.

2.7.3. Histological analysis of SCC

Fixed tumor tissues were carefully embedded in paraffin, and 5 μm-thick histological sections were prepared onto slides using a microtome (Leica, Hessen, Germany). After deparaffinization and rehydration, the tissues underwent hematoxylin and eosin (H&E) staining. The resulting H&E-stained sections were analyzed using an Axiovert microscope (Axioplan, Carl Zeiss, North Rhine-Westphalia, Germany). Images were recorded using a Zeiss *Axiocam* color CCD *camera* and the AxioVision 4.8.2 software (Carl Zeiss, North Rhine-Westphalia, Germany).

2.8. DOX quantification assay by HPLC

DOX quantification from SLN, skin, and receptor solution was performed by HPLC system LC10-AD (Shimadzu, Kyoto, Japan) equipped with an LC-10AT binary pump, a SIL-10AD autosampler, a CTO-10 SA column oven, RF-10AX fluorescence detector (λexc 480/ λem 560 nm), using a previously validated method by our research group (Taveira et al., 2012). A Lichorosphere 100 RP-18 (5 μm × 125 mm × 4 mm) column and guard column (5 μm × 10 mm × 4 mm) operated at 35 °C were employed with a mobile phase composed of phosphate buffer (50 mM, pH 2): acetonitrile: isopropanol (65:25:2, v/v/v), a flux of 1 mL. min^{-1}, and injection volume of 100 μL.

2.9. Statistical analysis

The *in vitro* results and the standardization of LFU-application time *in vivo* were analyzed via one-way ANOVA, with Tukey's post hoc test ($p < 0.05$ was considered the minimum significance value). DOX skin penetration and SCC-treatment *in vivo* studies were analyzed by two-way ANOVA, with Bonferroni's post hoc test ($p < 0.05$ was considered the minimum significance value).

3. Results and discussion

3.1. Formulation selection and experimental protocols for in vitro and in vivo studies with LFU

DOX is an antineoplastic drug of the anthracycline class widely used to treat solid tumors. To mitigate the toxic effects associated with systemic administration, researchers have explored DOX potential for topical treatment of skin tumors (Huang et al., 2020; Wang et al., 2013; Herai et al., 2007; Taveira et al., 2009). However, the hydrophilic nature of DOX poses a challenge to its skin penetration when applied in its free form (Herai et al., 2007; Taveira et al., 2009). Encapsulation of DOX in NLS has shown promising results by enhancing its skin penetration (Taveira et al., 2014; Huber et al., 2015), decreasing DOX interactions with the SC and increasing its cytotoxicity against cutaneous melanoma cells (B16F10) (Taveira et al., 2012) and SCC (Taveira et al., 2014).The formulation of SLN used in this study was based on our previously published works (Taveira et al., 2012; Huber et al., 2015), where the nanoparticles were extensively characterized. In brief, the ratio of components was determined by constructing pseudo-ternary phase diagrams to identify the region of microemulsion formation, which is essential for SLN production. The selection of the oily phase was guided by considering the melting temperature of the stearic acid and the stabilizers, monoolein and CTAB, considering their individual properties. CTAB, a surfactant with antimicrobial properties that safeguard formulations against contamination, has been demonstrated to enhance skin drug penetration effectively (Shokri et al., 2001; Nokhodchi et al., 2003). Monoolein, a polar lipid, facilitates the interaction of DOX with the skin, thereby promoting its skin penetration (Herai et al., 2007). Furthermore, depending on its concentration, monoolein can form various crystalline mesophases when in contact with water (Milak and Zimmer, 2015), contributing to the enhanced stability of the SLN dispersion (Chen et al., 2010; Huber et al., 2015).

The experimental conditions for LFU pretreatment of the skin were carefully selected based on the existing literature and our previous research findings. Similar LFU parameters have been widely used in other studies employing LFU to permeabilize the skin (e.g., Polat et al., 2011b). Moreover, we have previously investigated the influence of hydrogel coupling media on the formation and distribution of LTRs on the skin (Pereira et al., 2017) using the same LFU protocol as in the current study. Given the established and proven effectiveness of these LFU parameters in promoting skin permeability and the consistent results obtained in our prior work, we considered them appropriate for this investigation.

In selecting the therapeutic regimen employed in our *in vivo* studies conducted on SCC-induced mice, it is essential to recognize the established intravenous dosing regimens for DOX in systemic cancer treatment. Typically, these regimens involve dosages ranging from 60 to 75 mg/m^2, administered as a single intravenous injection with intervals of 21 days between doses (Sledge et al., 2003). However, it is crucial to emphasize that the intravenous dosing regimen is tailored explicitly for systemic therapy and is not directly applicable to our localized, topical approach utilizing LFU for treating skin tumors.

Our research is fundamentally centered on exploring the potential of this innovative topical treatment method. We aim to investigate how specific formulation characteristics and the distance of the ultrasound transducer from the skin surface influence the treatment outcomes. Given the unique nature of our approach, it necessitated an adjustment to the dosage regimen.

Drawing insights from prior studies on DOX topical treatments, we observed significant variations in effective dosages. For example, daily topical administration of 120 – 240 μg/Kg for 40 days of SLN-DOX on B16F10 tumors in a similar animal model, as used in the present study, inhibited tumor growth (Tupal et al., 2016). Furthermore, in our previous research, which involved topical administration via iontophoresis, we applied 76 mg/Kg of SLN-DOX for 30 min to SCC-induced mice every 3 days, totaling 5 treatments, with an evaluation of tumor growth rates conducted after 21 days (Huber et al., 2015). In this study, we observed a 3.5-fold reduction in growth rate compared to the control group, alongside a decrease in undifferentiated cells and increased keratinization.

In our current study, the chosen therapeutic regimen of daily topical application of 6 mg/Kg of DOX-nanogel after LFU pretreatment, conducted every 3 days for a total of 5 treatments, has been tailored to align with the distinct requirements of our topical approach, minimizing systemic exposure. Furthermore, it fulfills the predefined objectives of

our *in vivo* study, which primarily focus on optimizing the experimental conditions in preparation for upcoming *in vivo* investigations.

3.2. Characterization of SLNs and nanogel formulations

Table 1 shows the physicochemical properties of the SLN and the nanogels prepared in the presence and absence of SLN.

The analysis of the nanogel and the nanogel-DOX by PCS allowed the observation of tiny nanoparticles in the 10 to 22 nm range. The size range of the SLN and the nanoparticle formulations was 100 – 200 nm. The SLN presented physicochemical characteristics similar to those previously reported and prepared with the same components and technique (Huber et al., 2015). Notably, no statistically significant difference in size was observed among the various SLN-based formulations, indicating that encapsulation or incorporation in the nanogel did not alter SLN size (Table 1). Other reports have also found no significant changes when polymeric (Shah et al., 2012) or lipid (Jain et al., 2014; Souto et al., 2004) nanoparticles were incorporated into hydrogels.

Regarding zeta potential, the SLN has a positive zeta potential due to the presence of the cationic surfactant, CTAB, while the nanogels showed a zeta potential close to neutrality (Table 1). Including the cationic SLN in the nanogel led to a positive shift in the zeta potential, making the SLN-nanogel cationic compared to the nanogel. Interestingly, encapsulating DOX within the SLN reduced the positive zeta potential of the SLN. This reduction could be attributed to the interactions between the components of DOX and SLN, which may lead to structural reorganization and subsequently affect the surface characteristics of the nanoparticles.

Remarkably, when both SLN and SLN-DOX were dispersed into the nanogel matrix, a more substantial decrease in the zeta potential of the SLN or SLN-DOX was observed (Table 1). The dispersion of poloxamers in water (nanogel) attempts to maintain the electro-neutrality of the system upon the addition of SLN, prompting a redistribution of counterions present on the surface of the nanoparticles. This redistribution affected the zeta potential. Therefore, the potential difference between the nanoparticles' surfaces and the bulk medium (nanogel) was reduced. In other words, the electrical charge difference between the nanoparticles and the surrounding medium becomes smaller.

It is worth noting that despite the decrease in zeta potential following the incorporation of SLN and SLN-DOX into the nanogel, the zeta potential remained significantly higher than that of the SLN-free nanogels. Moreover, these alterations in charge distributions did not significantly change the encapsulation efficiency of DOX in the SLN, which remained in the range of 45–50%, corroborating with another paper of our group that prepared similar SLN-DOX (Huber et al., 2015).

Table 1
Physicochemical characteristics of SLN and nanogels.

Formulation	Particle size (nm)	PdI	Zeta potential (mV)	EE (%)
Nanogel	13 (±2)	0.33 (±0.12)	5 (±2)	–
Nanogel-DOX	17 (±5)	0.25 (±0.06)	1 (±2)	–
SLN	221 (±40)*	0.28 (±0.02)	68 (±7)*	–
SLN-DOX	136 (±17)*	0.29 (±0.02)	56 (±0)*#	47 (±2)
SLN-nanogel	173 (±7)*	0.23 (±0.02)	12 (±0)*#$	–
SLN-DOX nanogel	197 (±40)*	0.20 (±0.04)	15 (±4)*#$	48 (±1)

The symbols above the numbers represented statistical differences within the same column when the differences between the means were analyzed by one-way ANOVA, with Tukey's post hoc test ($p < 0.05$): *Significantly different from nanogel and nanogel-DOX, #Significantly different from SLN, $Significantly different from SLN-DOX.

Fig. S1 in the supplementary material shows a representative AFM image of the SLN-DOX in a dry state. It is possible to observe quasi-spherical structures with 70 ± 13 nm of diameter. However, the nanoparticles' size was about twice as small as that determined by PCS (Table 1). This can be attributed to the differences between the radius of the nanoparticles measured in the dry and hydrated states in the AFM and PCS analysis, respectively. Moreover, the attractive forces with the support and the cantilever tapping against the sample could induce changes to the soft nanoparticles during the surface scanning. These findings agree with other studies (Scioli Montoto et al., 2018).

In the polarized light microscopy, SLNs and SLN-nanogel showed birefringence, while the nanogel was isotropic (Supplementary material, Fig. S2). Therefore, the addition of SLN to the nanogel altered the structural organization of the gel. The isotropic appearance of the nanogel was of cubic crystalline phases, which was confirmed by the SAXS analysis (Table 2). Upon incorporating the SLN into the nanogel, traces of the birefringence previously observed in the SLN were still apparent.

Table 2 shows diffractogram data of the SAXS analysis and the crystalline structures present in the formulations. The nanogel exhibited cubic liquid crystals, while the birefringence observed in the polarized light microscopy of SLN corresponded to the presence of lamellar liquid crystals. The DOX encapsulation in the SLN could not disrupt the liquid crystalline organization, and the lamellar structure of the blank SLN was maintained in SLN-DOX (a = 4.02). As previously reported (Clogston et al., 2000; Petrilli et al., 2016), monoolein dispersions in water have been shown to form lamellar crystalline structures. Consequently, the lamellar phase observed in the SLN dispersions could be attributed to the monoolein organization in the nanoparticles' surface. The discernible presence of unique liquid crystalline phases between the free SLN nanogel and the SLN led to the identification of a coexistence of lamellar and cubic phases within the SLN-nanogel and SLN-DOX nanogel formulations (Table 2).

The addition of SLN in the nanogel increased the lattice parameter from approximately 20 to 23 nm (Table 2). However, incorporating SLN-DOX into the nanogel decreased the lattice parameters compared to SLN-nanogel.

The lattice parameter is related to the internal arrangement of the liquid-crystalline phase and offers valuable insights into the distances between the nuclei of micelles organized within the gel (Amar-Yuli

Table 2
SAXS analysis of SLN and nanogel formulations and the liquid crystalline structures observed.

Parameter	SLN	SLN-DOX	Nanogel	SLN-nanogel	SLN-DOX nanogel
q (nm^{-1})	1.56 (peak 1) 3.11 (peak 2)	1.56	0.31 (peak 1) 0.63 (peak 2)	0.27 (peak 1) 0.55 (peak 2) 1.56 (peak 3)	0.31 (peak 1) 0.63 (peak 2) 1.56 (peak 3)
d (nm)	4.02 (peak 1) 2.02 (peak 2)	4.02	20.08 (peak 1) 10.00 (peak 2)	23.25 (peak 1) 11.42 (peak 2) 4.02 (peak 3)	20.08 (peak 1) 10.04 (peak 2) 4.02 (peak 3)
Ratio	1:1 (peak 1) 1:1/2 (peak 2)	1:1	1:1 (peak 1) 1:$\sqrt{4}$ (peak 2)	1:1 (peak 1) 1:$\sqrt{4}$ (peak 2) 1:1 (peak 3)	1:1 (peak 1) 1:$\sqrt{4}$ (peak 2) 1:1 (peak 3)
Mean lattice parameter - a (nm)	4.02 (peak 1) 4.04 (peak 2)	4.02	20.04 (peak 1) 20.00 (peak 2)	23.25 (peak 1) 22.85(peak 2) 4.02 (peak 3)	20.08 (peak 1) 20.08(peak 2) 4.02 (peak 3)
Structure	Lamellar	Lamellar	Cubic	Cubic/ Lamellar	Cubic/ Lamellar

et al., 2007). Incorporating blank SLN into the nanogel (SLN-nanogel) increased the lattice parameter of the nanogel, implying that the nanoparticles might be situated within the inner core of the nanogel's liquid crystalline structure (Libster et al., 2009). However, the lattice parameter of the SLN-DOX nanogel was smaller than that of the SLN-nanogel, suggesting that the free DOX present in the SLN-DOX, approximately 50% (Table 1), could have competed with both the nanogel-forming poloxamer and the SLN for the water. This dehydration effect, resulting from the presence of a drug in a liquid crystalline dispersion, aligns with previous observations and has been shown not to impair the cutaneous permeabilization potential of liquid crystalline structures (Petrilli et al., 2013).

The formulations' different compositions and structural organizations can impact on viscosity, influencing the drug release and cavitation process from LFU application (Pereira et al., 2017). The rheological behavior of nanogel and SLN-DOX nanogel at 25 ± 1 °C is presented in the Supplementary material (Fig. S3). Under the conditions used in this work, the nanogels were already semisolid (gelled) at this temperature. As expected, the nanogels presented a non-Newtonian pseudoplastic behavior with flow indices of 0.946 and 0.962 for nanogel and nanogel-containing lipid nanoparticles, respectively.

Using the experimental data shown in the rheogram of Fig. S3 (Supplementary material) and based on the Herschel-Bulkley model, the apparent viscosity of the nanogel and SLN-DOX nanogel was calculated at a shear rate of 100 s^{-1}, yielding values of approximately 4.5 Pa.s and 2.1 Pa.s for the nanogel and SLN-DOX nanogel, respectively.

Adding SLN-DOX to the nanogel reduced the nanogel's apparent viscosity (Fig. S3). This phenomenon can be understood by considering the principles of the rheological behavior of dispersions and the influence of particle size. Small particles, such as those comprising the nanogel (approximately 15 nm, Table 1), exhibit more pronounced Brownian motion due to random thermal agitation, which hinders their alignment in the direction of flow. This behavior contributes to a higher apparent viscosity, requiring a higher shear rate to overcome Brownian motion and enable particle alignment. Incorporating SLN-DOX, which contains substantially larger particles (approximately 150 nm, Table 1), reduces the prominence of Brownian motion. Larger particles experience less thermal agitation, making them more likely to align in the direction of flow with less resistance. This more efficient particle alignment results in a reduction in the apparent viscosity of the dispersion. This phenomenon aligns with previous observations (Silva et al., 2012), which identified a correlation between particle size and the viscosity of hydrogels.

A critical property of the formulations that can impact the formation of LFU-induced LTR on the skin is the surface tension of the coupling medium (Pereira et al., 2017). Consequently, the surface tension of the SLN, nanogel, and SLN-nanogel used as coupling mediums for skin LFU pretreatment was determined (Table 3). Additionally, for comparative purposes, the surface tension value of a PBS solution containing 1% sodium lauryl sulfate (SLS), a widely utilized coupling medium in LFU skin pretreatments (Tezel et al., 2002; Lopez et al., 2011; Polat et al., 2011a) is also presented in Table 3.

SLN exhibited the lowest surface tension, followed by the SLS, nanogel, and then the SLN-nanogel (Table 3). The surface tension of the coupling medium is a relevant factor that determines the behavior of acoustic microbubbles generated by LFU, impacting their size and collapse dynamics (Kuvshinov, 1991). Higher surface tension leads to reduced expansion and increased compression rates of microbubbles, resulting in more violent collapses against the skin surface (Polat et al., 2011a).

Table 3
Surface tension of coupling mediums used at 25 ± 2 °C in skin pretreatment with LFU.

Coupling Medium	Surface Tension ($mN.m^{-1}$)
SLS	35.9 (±0.1)[Pereira et al., 2011]
SLN	30.5 (±0.1)[a]
Nanogel	41.6 (±0.4)[b]
SLN-nanogel	50.2 (±1.3)[c]

Values with different letters (a, b, c) indicate statistically significant differences (one-way ANOVA, with Tukey's post hoc test, $p < 0.05$).

The addition of surfactants to an aqueous medium decreases its surface tension. For instance, the coupling medium with 1% SLS exhibits a surface tension of approximately 36 $mN.m^{-1}$, about two times lower than that of water (73.3 $mN.m^{-1}$, at 25 °C) (Pereira et al., 2017). Notably, Table 3 reveals that the surface tension of SLN, although resembling the macroscopic fluidity of water, is even lower than that of SLS. This outcome could be attributed to the presence of the cationic surfactant CTAB in the SLN composition and the co-surfactant monoolein. These agents may have synergistically contributed to reducing the interfacial tension of SLN, resulting in its low surface tension.

Among the viscous coupling media, the addition of SLN, which significantly reduced the surface tension of water, led to an increase in the surface tension of the nanogel instead of a decrease. The incorporation of SLN into the semisolid formulation altered the structural organization of the nanogel, as observed in the results of the SAXS analysis (Table 2). This modification changed the interfacial properties of the nanogel and counterbalanced the surface tension-reducing effect caused by the SLN components. Additionally, the interaction between the surfactants in the SLN and the nanogel matrix might have played a crucial role. This intricate interplay between the SLN components and the nanogel likely contributed to the observed increase in surface tension.

3.3. Skin LFU pretreatment: effects of nanoparticulate coupling media on skin LTR distribution

It is widely recognized that alterations in the LFU coupling medium can potentially modify the distribution of the LTR within the skin (Pereira et al., 2017). Consequently, these modifications hold the potential to impact the depth to which a drug can permeate the skin upon direct contact. This underscores the importance of conducting a thorough assessment of the impact of the studied nanoparticulate systems – namely nanogel, SLN, and the SLN-nanogel combination – on the distribution of LTR within the skin.

Fig. 1 presents images of skin samples subjected to LFU treatment with distinct coupling media (SLN, nanogel, and SLN-nanogel). The regions shaded in red correspond to the LTR labeled with Allura red. Specifically, the quantification reveals that the percentage of skin area encompassing LTR is measured at 26 ± 24% for SLN, 55 ± 21% for nanogel, and 54 ± 19% for SLN-nanogel coupling media applications.

The coupling medium with the lowest surface tension and viscosity, the SLN formulation, formed the smallest LTR area on the skin after LFU application. As shown in Fig. 1, this coupling medium generated discrete, small-sized LTR spread across a substantial portion of the skin surface. In contrast, employing SLS as the coupling medium, with the same LFU parameters, exhibited a pattern of accumulated LTR in a specific region of the skin, covering 11 ± 17% of the skin area, as reported before by our research group (Pereira et al., 2017).

It is recognized that when acoustic microbubbles collapse near solid surfaces, they generate high-speed (~100 $m.s^{-1}$) liquid microjets (Wolloch and Kost, 2010). The lower surface tension of the SLN-coupling medium (Table 3) may have decreased the size and increased the number of acoustic microbubbles compared to the SLS-coupling medium, causing a decentralization of the microjets. This alteration is believed to be responsible for the observed pattern shift in the LTR distribution on the skin surface. This shift in LTR distribution can potentially influence drug penetration into the skin.

Moreover, it is essential to note that the components of the coupling medium can penetrate the skin in the presence of LFU, which could lead to changes not only in the LTR but also in other skin areas where the components penetrate—for instance, pretreating the skin with LFU

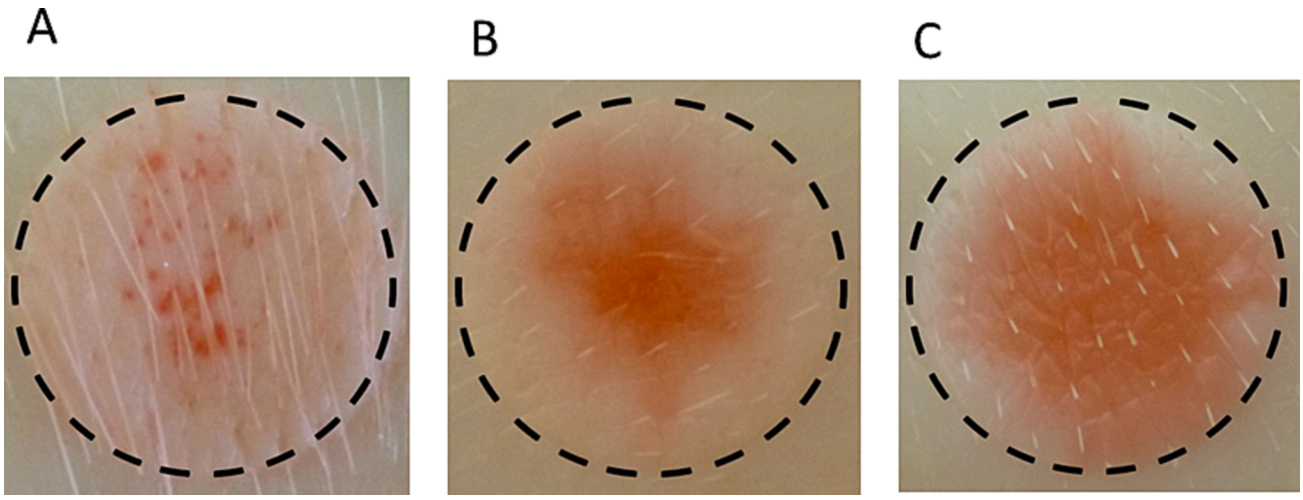

Fig. 1. Representative images depicting the LTR stained with Allura red developed on the skin following treatment with LFU using different coupling mediums: A) SLN, B) Nanogel, C) SLN-nanogel. LFU parameters: 20 kHz, I_{sata} of 9.6 ± 0.5 W/cm^2, and 50% duty cycle (5 s on, 5 s off). The skin samples underwent LFU treatment until achieving a resistivity of 0.7 ± 0.2 KΩ.cm^2.

using SLS as the coupling medium induces two distinct levels of heightened skin permeability (Polat et al., 2011b). The more significant increase occurs within the LTR. The subsequent smaller increase occurs in non-LTR due to the disorganization caused by the penetration of SLS into the skin areas adjacent to LTR. In this context, prior studies have demonstrated that pretreating the skin with LFU-SLS resulted in comparable levels of DOX in the skin to that skin pretreated with neutral hydrogels as coupling mediums. This similarity was observed even though approximately 50% of the skin surface was covered by LTR in the LFU-hydrogel pretreatment, against only 10% in the case of LFU-SLS pretreatment (Pereira et al., 2017).

In this sense, the surfactants in SLN, CTAB and monoolein, also known as skin penetration enhancers (Nokhodchi et al., 2003; Herai et al., 2007), can potentially elevate skin permeability. However, SLN could also be driven into LTR upon LFU exposure, potentially altering skin composition. Indeed, studies have demonstrated that fatty formulations, combined with LFU, can repair skin disrupted by LFU due to their ability to penetrate the skin (Dahlan et al., 2009; Essa et al., 2004).

Therefore, a comprehensive evaluation was undertaken to examine the extent of DOX penetration into skin pretreated with SLN, nanogel, and SLN-nanogel, as elaborated in the subsequent section. Furthermore, acknowledging the potential impact of the formulation composition in contact with the pretreated skin on drug penetration, an additional investigation was initiated, as outlined in the following section, aiming to elucidate the influence of both the hydrophilic nanoparticulate system, DOX-nanogel, and its lipophilic counterpart, SLN-DOX nanogel, on the effectiveness of topically administering DOX to LFU-pretreated skin.

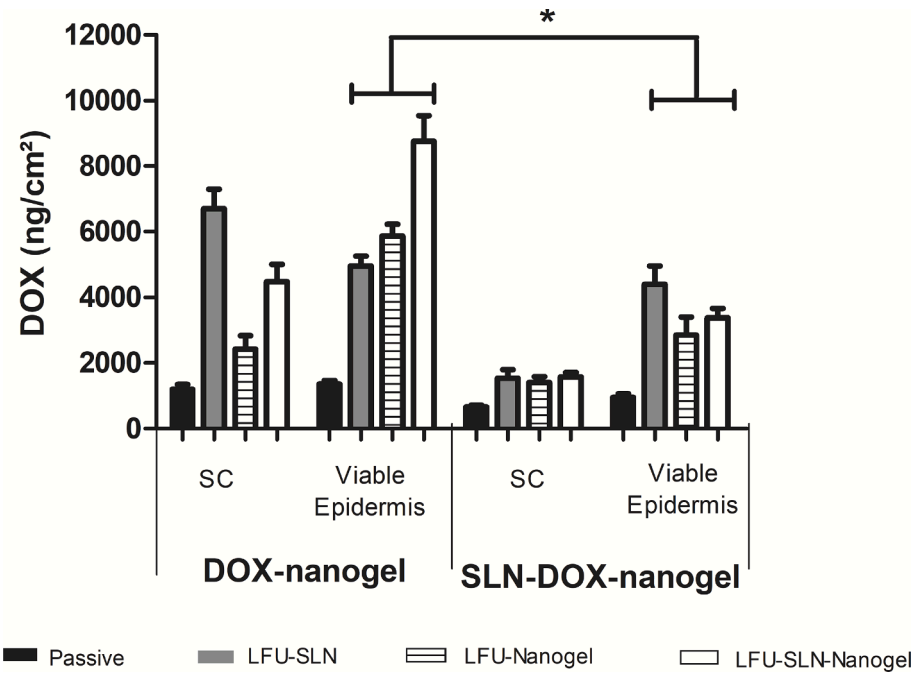

Fig. 2. DOX recovered from the SC and viable epidermis after 26 h of treatment with DOX-nanogel or SLN-DOX nanogel formulations. "Passive" denotes skin treated with DOX formulations without LFU pretreatment. "LFU-SLN," "LFU-Nanogel," and "LFU-SLN-nanogel" correspond to skin that underwent LFU pretreatment using SLN, nanogel, and SLN-nanogel as coupling mediums. The data is the mean ± standard deviation (n = 6). Statistical analysis involved a two-way ANOVA followed by post hoc analysis employing Bonferroni's test, with a significance level set at $p < 0.05$.

3.4. Nanoparticle-mediated enhancement of DOX penetration through LFU-permeabilized skin

Fig. 2 shows DOX recovered from the SC and viable epidermis after skin pretreatment with LFU using SLN, nanogel, or SLN-nanogel as coupling mediums followed by skin treatment with DOX-nanogel or SLN-DOX nanogel compared to non-LFU pretreatment (passive treatment).

The penetration of DOX into the viable epidermis was comparable after exposure to the DOX-nanogel and SLN-DOX nanogel formulations when the skin was not subjected to LFU pretreatment (passive) (*t*-test, $p > 0.05$). However, pretreatment of the skin with LFU significantly enhanced the penetration of DOX in all experimental scenarios (as determined by two-way ANOVA followed by post hoc analysis using Bonferroni's test, with a significance level set at $p < 0.05$).

Within the viable epidermis, DOX quantified after LFU pretreatment was remarkably higher than the passive treatment (Fig. 2). As skin tumors are sited in the epidermis layer, higher DOX concentration up this layer is essential to secure drug uptake by the target cells. Thus, for *in vitro* penetration studies, the more significantly the drug accumulated in deeper layers of the skin, the better evidence that the drug could reach tumor cells at therapeutic levels.

Although the SLN-LFU pretreatment of the skin resulted in a lower area of LTR than the pretreatment with the nanogel (Fig. 1), DOX penetration in the viable epidermis was similar to that observed when the nanogel was used as coupling media (Fig. 2). Therefore, no significant distinction was observed in the DOX accumulation attributed to the coupling medium employed during LFU pretreatment.

However, the formulation with which the skin was treated after LFU pretreatment, the one that carried the DOX by the LFU permeabilized skin, clearly altered the DOX penetration. As shown in Fig. 2, subsequent treatment of LFU-pretreated skin with DOX-nanogel yielded notably higher levels of DOX within the skin compared to treatment with SLN-DOX nanogel.

It is essential to highlight that the presence of DOX in the receptor medium was not quantified following any of the administered treatments.

Previous studies showed that free DOX strongly interacts with the SC (Herai et al., 2007) and that SLN can target DOX to the viable epidermis (Huber et al., 2015; Taveira et al., 2012). However, the sonophoretic transport of the drug to the viable epidermis from SLN-DOX nanogel was two times lower than that from the DOX-nanogel. This lower penetration can be attributed to the high lipids content of the SLN, which could repair the LTR during its diffusion and reduce the DOX transport to the viable epidermis.

Therefore, the content of lipids and surfactants of lipid-based nanoparticles play an essential role in the sonophoretic transport of drugs. For instance, it was previously demonstrated that the association of LFU with DSPE-PEG polymeric micelles (Martins et al., 2020) and Labrasol and Transcutol microemulsion (Quiroz-Segoviano et al., 2019) led to enhanced penetration of photosensitizing agents for skin cancer treatment. In these cases, although the role of the formulation components on the skin penetration of the photosensitizers was not analyzed, the low lipid content of the micellar system and high concentration of surfactants of the microemulsion should keep the hydrophilic channels of the LTR open.

In this sense, in our study, the hydrophilic nanogel could have protected DOX from direct contact with the SC, not altering LTR's hydrophilic nature and dispatching the drug molecules to the viable epidermis via LTR. Due to their nanoparticle nature, these hydrophilic nanogels also offer the advantage of potentially sustaining and controlling the delivery of DOX within the skin. This localized approach holds promise in minimizing the risk of undesired systemic effects often associated with widespread drug circulation in the body.

Consequently, our findings suggest that the hydrophilic nanogel is a suitable nanoparticulate platform for LFU-mediated transport of DOX. In contrast, treating the LFU-permeabilized skin with the lipid nanoparticle SLN-DOX aiming for high drug concentration in a skin tumor seems unsuitable due to the counterproductive impact of SLN on LTR restoration.

In summary, the *in vitro* study using porcine ear skin provided valuable insights into the impact of different coupling media on LTR formation and the influence of nanoparticle-based formulations on drug penetration following LFU pretreatment. Porcine skin is a well-established alternative to human skin in permeation studies, offering comparable SC thickness, lipid composition, and barrier properties (Hwang et al, 2021).

3.5. Exploring the potential of LFU-nanoparticle association in tumor treatment through in vivo studies and experimental protocol variations

In our *in vivo* investigations, our primary focus was assessing the potential of LFU-nanoparticle association in tumor treatment and elucidating the influence of the experimental protocol on achieving the desired therapeutic outcomes. To this end, we developed a protocol for *in vivo* pretreatment of skin tumors using LFU. Additionally, we showcased the impact of altering the distance between the ultrasound tip and the tumor surface on the subsequent treatment response.

To facilitate this evaluation, we employed a BALB/c nude mouse model in which SCC was induced using human tumor cells (A431 cells). This well-established xenograft model is widely utilized to study human cancer biology and assess emerging therapeutic approaches (Petrilli et al., 2018; Dalmolin and Lopez, 2018). The utilization of immunosuppressed mice offered a controlled and relevant environment for examining both tumor growth and treatment response.

3.5.1. Evaluating in vivo skin electrical resistivity and LFU application time for tumor permeabilization

Many LFU studies have investigated the skin's electrical resistivity under ultrasound exposure. This assessment holds immense significance because the extent of cutaneous permeabilization achieved does not exhibit a straightforward correlation with the LFU's application time. This discrepancy can be attributed to variations in the skin's mechanical properties when prepared on the diffusion cell for *in vitro* treatment and the integrity of the dissected SC (Karande et al., 2006; Seto et al., 2010). Previously, *in vivo*, LFU investigations involved determining skin resistivity by subcutaneously implanting an Ag/AgCl electrode in the dorsal region near the head of mice (Tang et al., 2002). However, due to the invasive nature of this technique, we standardized a non-invasive method for assessing *in vivo* skin resistivity, as described in the methods (Section 2.7.1). This technique entails affixing a patch containing an Ag/AgCl electrode to the mouse's tail, a strategy frequently utilized as a counter electrode in iontophoresis studies (Gelfuso et al., 2011).

To validate our approach, after determining the resistivity of healthy mouse skin *in vivo*, the area of skin that underwent LFU was dissected and mounted in a diffusion cell to determine its resistivity *in vitro*. The electrical resistivity of the mouse skin, measured non-invasively after a 1-minute LFU treatment *in vivo* and *in vitro*, is presented in the Supplementary material (Table S1). The non-invasive *in vivo* protocol yielded results comparable to the *in vitro* determination, thus enabling its convenient utilization in assessing alterations in skin electrical resistivity resulting from LFU application *in vivo*.

However, following the 1-minute LFU treatment, the resistivity of the healthy mouse skin was measured at 2.9 ± 0.2 kΩ.cm^2, which is three times higher than the desired target of 1 kΩ.cm^2. It is worth noting that the standardized application time consistently yielded reproducible values across the different mice utilized in the study.

To determine the optimal number of LFU cycles needed to achieve a skin resistivity close to 1 kΩ.cm^2, the electrical resistivity of the healthy mice skin was continuously monitored *in vivo*. This monitoring took place following each cycle of the LFU application, where each cycle

consisted of 5 s of LFU exposure followed by 5 s of rest. The results revealed that an average of 3 ± 1 cycles, equivalent to approximately 15 s of LFU exposure, was necessary to attain the desired electrical resistivity level of around 1 kΩ.cm^2.

At the outset, an identical protocol was implemented for LFU permeabilization of tumors developed in mice. However, visible lesions emerged on the tumor surface after undergoing 3 to 4 complete cycles of 5 s each (5 s ON, 5 s OFF) of treatment. Furthermore, even with 5 complete cycles of LFU (25 s of exposure), the preset resistivity threshold (1 kΩ.cm^2) remained unattained. This phenomenon can be attributed to the hyperkeratinization of the tumor. Excess keratin hinders the passage of electrical current through the skin, resulting in elevated electrical resistivity values even when the tumor is already modified by ultrasound. Consequently, it was decided to standardize the number of LFU application cycles to avoid harming the animals' skin instead of relying solely on resistivity measurements. Therefore, the decision was to administer LFU treatment for 2 complete cycles of 5 s each, totaling 10 s of LFU exposure, corresponding to 20 s of pretreatment.

3.5.2. *The influence of LFU tip positioning relative to tumors surface on topical DOX-nanogel treatment for skin tumors*

Fig. 3 shows tumor volume as a function of time for groups of animals treated with DOX-nanogel passively or after pretreatment with LFU positioned at different distances from the skin.

Animals that were not pretreated with the LFU but received daily topical application of the DOX-nanogel did not present significant tumor regression in comparison to the control ($p > 0.05$) (which did not receive any treatment) (Fig. 3A). Pretreatment of the skin with LFU-nanogel before the daily application of the DOX-nanogel led to different and exciting results depending on the distance at which the LFU tip was positioned from the tumor surface. At 5 mm from the tumor surface (5 mm-LFU), pretreatment with LFU-nanogel did not suppress tumor growth (Fig. 3B). Positioning the LFU tip 10 mm from the tumor surface (10 mm-LFU) significantly inhibited tumor growth. After 21 days of treatment with the LFU tip placed at 10 mm from the tumor surface, the tumor volume was approximately 6 times smaller than that of the control group.

The histological sections of the tumors 21 days after the start of treatment can be seen in Fig. 4. The passive treatment group (mice treated daily with DOX-nanogel) yielded a significant loss of tumor cells. It increased necrotic areas and keratin production compared to the control group (without treatment). The pretreatment of the skin with 10 mm-LFU and 5 mm-LFU followed by DOX-nanogel administration also promoted the loss of tumor cells associated with an intense necrotic process, which was more potent when the ultrasound was applied from 10 mm of the skin surface.

Although the histological analysis of the passive treatment of tumors with DOX-nanogel showed a reduction in the size of tumor cells (Fig. 4), it did not cause a significant reduction in tumor size (Fig. 3A). Therefore, it seems that the amount of DOX penetrated without the LFU pretreatment was insufficient to kill a relevant number of cells and impact the tumor's growth rate.

The LFU pretreatment, on the other hand, noticeably showed that the distance at which the probe is positioned from the tumor surface impacts the treatment. At 10 mm from the surface, pretreatment with the LFU followed by applying the formulation reduced the tumor growth rate by over 4 times (Fig. 3B) and caused necrosis of the cancerous cells (Fig. 4). However, as in passive treatment, tumor growth reduction was not seen when the LFU tip was closer to the tumor surface.

Considering the ultrasound wavelength (λ) in water at 20 kHz measures 7.5 cm, the first pressure antinode, that is, the point where the wave pressure is maximum, is approximately 1.9 cm (λ/4) from the source (Polat et al., 2011a). Thus, the ultrasound positioned 10 mm from the skin is 0.9 cm away from the first antinode, while the one positioned 5 mm from the skin is 1.4 cm away, meaning it is farther from the first antinode.

When positioned closer to the first antinode pressure, the heightened pressure exerted by the wave enhances the efficiency of acoustic cavitation bubble forces in the skin, leading to increased tumor permeabilization. This phenomenon explains the superior results observed in tumor cell destruction with the 10-mm tumor-to-LFU tip distance treatment. However, to confirm the extent of DOX penetration, *in vitro* experiments with the transducer positioned at a 10 mm distance need to be conducted and compared to those obtained with a 5 mm probe distance. Nonetheless, our results suggest that increasing the LFU distance to 19 mm from the tumor would likely result in higher treatment efficiency due to its alignment with the first pressure antinode.

Overall, these experiments underscore the importance of LFU positioning for topical tumor permeabilization followed by DOX administration.

4. Conclusion

In conclusion, our study demonstrated the potential of hydrophilic nanogels as an effective platform for LFU-mediated DOX transport in skin tumor treatment. In contrast, lipid nanoparticles, such as SLN, restore the previous LFU-permeabilized skin regions. Our *in vivo* investigations highlighted the critical role of LFU positioning, with superior tumor cell destruction observed at a 10-mm distance from the tumor surface compared to 5 mm.

Overall, these findings emphasize the importance of optimizing nanoparticle-based formulation and LFU experimental protocol for

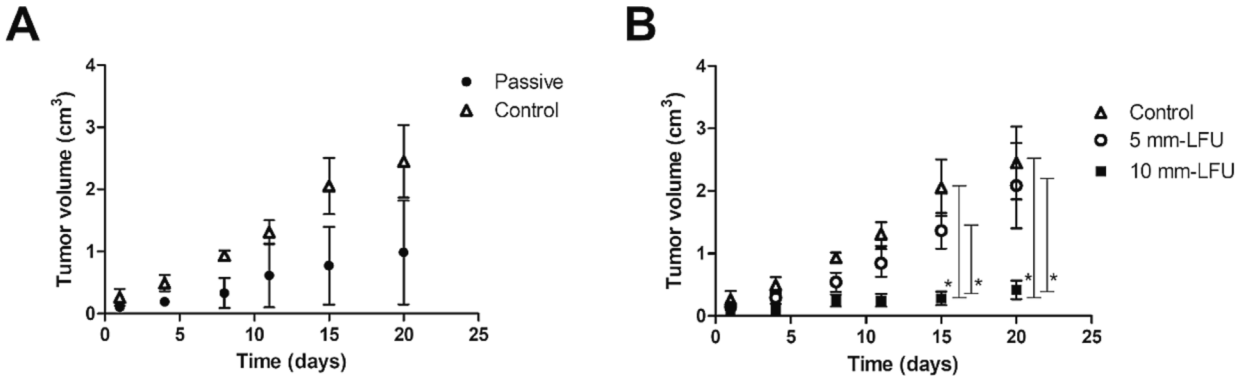

Fig. 3. Inhibitory effect of DOX-nanogel on tumor growth after LFU pretreatment. A) without pretreatment with LFU: (Δ) control group, which did not receive any treatment, (●) passive topical application of the DOX-nanogel. B) pretreatment with LFU-nanogel followed by application of the DOX-nanogel: (Δ) control group, (○) LFU tip positioned at 5 mm from the tumor surface (■) LFU tip positioned 10 mm from the surface of the tumor. * $p < 0.05$ analyzed by two-way ANOVA, with Bonferroni's post hoc test ($p < 0.05$ was considered the minimum significance value).

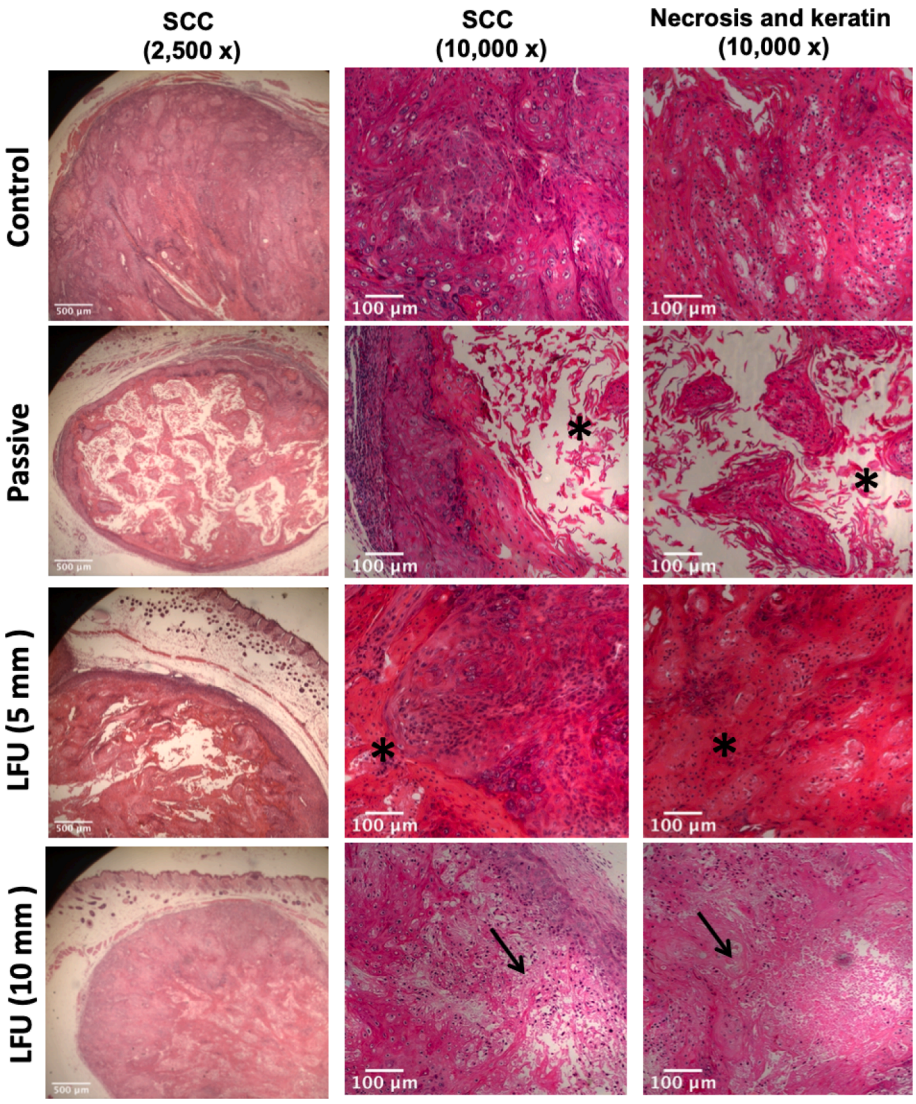

Fig. 4. Histopathology of SCC tumors following 21 days of treatment. The images provide representative samples from the Control, Passive, 5 mm-LFU, and 10 mm-LFU groups. DOX-nanogel was administered to the Passive and LFU groups (post-LFU treatment). (*) indicates keratin accumulation. Arrows indicate regions of necrosis. For images at 2,500x magnification (column 1) and 10,000x magnification (columns 2 and 3), the scale bars are 500 μm and 100 μm, respectively.

localized skin tumor treatment, offering promising prospects for clinical applications with reduced systemic side effects.

Funding

This research was sponsored by the São Paulo Research Foundation (FAPESP grants #2014/22451-7 and #10/20794-3), the National Institute of Science and Technology in Pharmaceutical Nanotechnology – INCT NANOFARMA (FAPESP grant number 2014/50928-2, and CNPq grant number 465687/2014-8), and the Coordination for the Improvement of Higher Education Personnel (CAPES 001).

CRediT authorship contribution statement

Tatiana Aparecida Pereira: Conceptualization, Investigation, Methodology, Validation, Formal analysis, Data curation, Visualization, Writing – review & editing. **Danielle Nishida Ramos:** Methodology, Validation, Investigation. **Lays Martin Sobral:** Methodology, Validation, Formal analysis, Data curation. **Yugo Araújo Martins:** Formal analysis, Writing – review & editing. **Raquel Petrilli:** Formal analysis, Writing – review & editing. **Márcia de Abreu Carvalho Fantini:** Formal analysis, Data curation. **Andréia Machado Leopoldino:** Formal analysis, Data curation. **Renata Fonseca Vianna Lopez:** Conceptualization, Methodology, Formal analysis, Supervision, Project administration, Funding acquisition, Resources, Writing – review & editing.

Declaration of Competing Interest

The authors declare that they have no known competing financial interests or personal relationships that could have appeared to influence the work reported in this paper.

Data availability

Data will be made available on request.

Acknowledgments

The authors would like to thank the Sao Paulo Research Foundation (FAPESP grant #2014/22451-7 and #10/20794-3) and the National Institute of Science and Technology in Pharmaceutical Nanotechnology – INCT NANOFARMA (FAPESP grant number 2014/50928-2, and CNPq grant number 465687/2014-8).

Appendix A. Supplementary data

Supplementary data to this article can be found online at https://doi.org/10.1016/j.ijpharm.2023.123431.

References

Amar-Yuli, I., Wachtel, E., Shoshan, E.B., Danino, D., Aserin, A., Garti, N., 2007. Hexosome and hexagonal phases mediated by hydration and polymeric stabilizer. Langmuir 23 (7), 3637–3645. https://doi.org/10.1021/la062851b.

Chen, C.C., Tsai, T.H., Huang, Z.R., Fang, J.Y., 2010. Effects of lipophilic emulsifiers on the oral administration of lovastatin from nanostructured lipid carriers: physicochemical characterization and pharmacokinetics. Eur. J Pharm. Biopharm. 74 (3), 474–482. https://doi.org/10.1016/j.ejpb.2009.

Cho, H., Jammalamadaka, U., Tappa, K., Egbulefu, C., Prior, J., Tang, R., Achilefu, S., 2019. 3D printing of poloxamer 407 nanogel discs and their applications in adjuvant ovarian cancer therapy. Mol. Pharm. 16 (2), 552–560. https://doi.org/10.1021/acs.molpharmaceut.8b00836.

Clogston, J., Rathman, J., Tomasko, D., Walker, H., Caffrey, M., 2000. Phase behavior of a monoacylglycerol: (Myverol 18–99K)/water system. Chem. Phys. Lipids 107 (2), 191–220. https://doi.org/10.1016/S0009-3084(00)00182-1.

D'Orazio, J., Jarrett, S., Amaro-Ortiz, A., Scott, T., 2013. UV radiation and the skin. Int. J. Mol. Sci. 14 (6), 12222–12248. https://doi.org/10.3390/ijms140612222.

Dahlan, A., Alpar, H.O., Murdan, S., 2009. An investigation into the combination of low frequency ultrasound and liposomes on skin permeability. Int. J. Pharm. 379 (1), 139–142. https://doi.org/10.1016/j.ijpharm.2009.06.011.

Dalmolin, L.F., Lopez, R.F.V., 2018. Nanoemulsion as a platform for iontophoretic delivery of lipophilic drugs in skin tumors. Pharmaceutics 10 (4), 1–18. https://doi.org/10.3390/pharmaceutics10040214.

Ebnesajjad, S., 2006. Surface Tension and Its Measurement, in: Surface Treatment of Materials for Adhesion Bonding. Elsevier, pp. 9–28. 10.1016/B978-081551523-4.50004-3.

Essa, E.A., Bonner, M.C., Barry, B.W., 2004. Electrically assisted skin delivery of liposomal estradiol; phospholipid as damage retardant. J. Control. Release 95 (3), 535–546. https://doi.org/10.1016/j.jconrel.2003.12.015.

Gelfuso, G.M., Gratieri, T., Souza, J.G., Thomazini, J.A., Lopez, R.F.V., 2011. The influence of positive or negative charges in the passive and iontophoretic skin penetration of porphyrins used in photodynamic therapy. Eur. J. Pharm. Biopharm. 77 (2), 249–1225. https://doi.org/10.1016/j.ejpb.2010.11.018.

Gratieri, T., Gelfuso, G.M., Rocha, E.M., Sarmento, V.H., de Freitas, O., Lopez, R.F.V., 2010. A poloxamer/chitosan in situ forming gel with prolonged retention time for ocular delivery. Eur. J. Pharm. Biopharm. 75 (2), 186–193. https://doi.org/10.1016/j.ejpb.2010.02.011.

Herai, H., Gratieri, T., Thomazine, J.A., Bentley, M.V.L.B., Lopez, R.F.V., 2007. Doxorubicin skin penetration from monoolein-containing propylene glycol formulations. Int. J. Pharm. 329 (1–2), 88–93. https://doi.org/10.1016/j.ijpharm.2006.08.021.

Hickey, G.L., Grant, S.W., Dunning, J., Siepe, M., 2018. Statistical primer: sample size and power calculations-why, when and how? Eur. J. Cardiothorac. Surg. 54 (1), 4–9. https://doi.org/10.1093/ejcts/ezy169.

Huang, S., Liu, H., Huang, S., Fu, T., Xue, W., Guo, R., 2020. Dextran methacrylate hydrogel microneedles loaded with doxorubicin and trametinib for continuous transdermal administration of melanoma. Carbohydr. Polym. 246, 1–12. https://doi.org/10.1016/j.carbpol.2020.

Huber, L.A., Pereira, T.A., Ramos, D.N., Rezende, L.C.D., Emery, F.S., Sobral, L.M., Leopoldino, A.M., Lopez, R.F.V., 2015. Topical skin cancer therapy using doxorubicin-loaded cationic lipid nanoparticles and iontophoresis. J. Biomed. Nanotechnol. 11 (11), 1975–1988. https://doi.org/10.1166/jbn.2015.2139.

Hwang, J.H., Jeong, H., Lee, N., Hur, S., Lee, N., Han, J.J., Jang, H.W., Choi, W.K., Nam, K.T., Lim, K.M., 2021. Ex vivo live full-thickness porcine skin model as a versatile in vitro testing method for skin barrier research. Int. J. Mol. Sci. 22 (2), 1–16. https://doi.org/10.3390/ijms22020657.

Jain, A.K., Jain, A., Garg, N.K., Agarwal, A., Jain, A., Jain, S.A., Tyagi, R.K., Jain, R.K., Agrawal, H., Agrawal, G.P., 2014. Adapalene loaded solid lipid nanoparticles gel: an effective approach for acne treatment. Colloids Surf. B Biointerfaces 121, 222–229. https://doi.org/10.1016/j.colsurfb.2014.05.041.

Jeswani, G., Paul, S.D., Ajazuddin, D., R.,, 2021. Design of vincristine sulfate loaded poloxamer in situ nanogel: formulation and in vitro evaluation. J. Drug Deliv. Sci. Technol. 61, 1–9. https://doi.org/10.1016/j.jddst.2020.102246.

Kang, H., 2021. Sample size determination and power analysis using the G*Power software. J. Educ. Eval. Health 18 (17), 1–12. https://doi.org/10.3352/jeehp.2021.18.17.

Karande, P., Jain, A., Mitragotri, S., 2006. Relationships between skin's electrical impedance and permeability in the presence of chemical enhancers. J. Control. Release 110 (2), 307–313. https://doi.org/10.1016/j.jconrel.2005.10.012.

Krishnan, V., Mitragotri, S., 2020. Nanoparticles for topical drug delivery: potential for skin cancer treatment. Adv. Drug Deliv. Rev. 1 (153), 87–108. https://doi.org/10.1016/j.addr.2020.05.011.

Kushner, J., Blankschtein, D., Langer, R., 2004. Experimental demonstration of the existence of highly permeable localized transport regions in low-frequency sonophoresis. J. Pharm. Sci. 93 (11), 2733–2745. https://doi.org/10.1002/jps.20173.

Kuvshinov, G.I., 1991. Effect of surface tension on the collapse of a cavitation bubble. J. Eng. Phys. 60, 34–37. https://doi.org/10.1007/BF00871608.

Libster, D., Aserin, A., Yariv, D., Shoham, G., Garti, N., 2009. Soft matter dispersions with ordered inner structures, stabilized by ethoxylated phytosterols. Colloids Surf. B Biointerfaces 74 (1), 202–215. https://doi.org/10.1016/j.colsurfb.2009.07.020.

Lopez, R.F., Seto, J.E., Blankschtein, D., Langer, R., 2011. Enhancing the transdermal delivery of rigid nanoparticles using the simultaneous application of ultrasound and sodium lauryl sulfate. Biomaterials 32 (3), 933–941. https://doi.org/10.1016/j.biomaterials.2010.09.060.

Martins, Y.A., Fonseca, M.J.V., Pavan, T.Z., Lopez, R.F.V., 2020. Bifunctional therapeutic application of low-frequency ultrasound associated with zinc phthalocyanine-loaded micelles. Int. J. Nanomed. 15, 8075–8095. https://doi.org/10.2147/IJN.S264528.

Mehnert, W., Mader, K., 2001. Solid lipid nanoparticles: production, characterization and applications. Adv. Drug Deliv. Rev. 47 (2–3), 165–196. https://doi.org/10.1016/s0169-409x(01)00105-3.

Milak, S., Zimmer, A., 2015. Glycerol monooleate liquid crystalline phases used in drug delivery systems. Int. J. Pharm. 478 (2), 569–587. https://doi.org/10.1016/j.ijpharm.2014.11.072.

Molavi, O., Ma, Z., Mahmud, A., Alshamsan, A., Samuel, J., Lai, R., Kwon, G.S., Lavasanifar, A., 2008. Polymeric micelles for the solubilization and delivery of STAT3 inhibitor cucurbitacins in solid tumors. Int. J. Pharm. 347 (1–2), 118–127. https://doi.org/10.1016/j.ijpharm.2007.06.032.

Mortensen, K., Brown, W., 1993. Poly(ethylene oxide)—poly(propylene oxide)—poly(ethylene oxide) triblock copolymers in aqueous solution. The influence of relative block size. Macromolecules 26 (16), 4128–4135. https://doi.org/10.1021/ma00068a010.

Nemes, Z., Steinert, P.M., 1999. Bricks and mortar of the epidermal barrier. Exp. Mol. Med. 31 (1), 5–19. https://doi.org/10.1038/emm.1999.2.

Nokhodchi, A., Shokri, J., Dashbolaghi, A., Hassan-Zadeh, D., Ghafourian, T., Barzegar-Jalali, M., 2003. The enhancement effect of surfactants on the penetration of lorazepam through rat skin. Int. J. Pharm. 250 (2), 359–369. https://doi.org/10.1016/s0378-5173(02)00554-9.

Patel, D., Kesharwani, R., Kumar, V., 2020. Etodolac loaded solid lipid nanoparticle based topical gel for enhanced skin delivery. Biocatal. Agric. Biotechnol. 29, 1–9. https://doi.org/10.1016/j.bcab.2020.101810.

Pereira, T.A., Ramos, D.N., Lopez, R.F.V., 2017. Hydrogel increases localized transport regions and skin permeability during low frequency ultrasound treatment. Sci. Rep. 7, 1–10. https://doi.org/10.1038/srep44236.

Petrilli, R., Eloy, J.O., Praça, F.S.G., Ciampo, J.O.D., Fantini, M.A.C., Fonseca, M.J.V., Bentley, M.V.L.B., 2016. Liquid crystalline nanodispersions functionalized with cell-penetrating peptides for topical delivery of short-interfering RNAs: a proposal for silencing a pro-inflammatory cytokine in cutaneous diseases. J. Biomed. Nanotechnol. 12 (5), 1063–1075. https://doi.org/10.1166/jbn.2016.2211.

Petrilli, R., Eloy, J.O., Saggioro, F.P., Deise, L.C., Souza, M.C.D., Dias, M.V.S., Da Silva, L. L.P., Lee, R.J., Lopez, R.F.V., 2018. Skin cancer treatment effectiveness is improved by iontophoresis of EGFR-targeted liposomes containing 5-FU compared with subcutaneous injection. J. Control. Release 10 (283), 151–162. https://doi.org/10.1016/j.jconrel.2018.05.038.

Petrilli, R., Lopez, R.F.V., 2018. Physical methods for topical drug delivery: concepts and applications. Braz. J. Pharm. Sci. 54 (spe), 1–19. https://doi.org/10.1590/s2175-97902018000001008.

Petrilli, R., Praça, F.S.G., Carollo, A.R.H., Medina, W.S.G., De Oliveira, K.T., Fantini, M.C. A., Neves, M.G.P.M.S., Cavaleiro, J.A.S., Serra, O.A., Iamamoto, Y., Bentley, M.V.L. B., 2013. Nanoparticles of lyotropic liquid crystals: a novel strategy for the topical delivery of a chlorin derivative for photodynamic therapy of skin cancer. Curr. Nanosci. 9 (4), 434–441. https://doi.org/10.2174/1573413711309040003.

Polat, B.E., Figueroa, P.L., Blankschtein, D., Langer, R., 2011a. Transport pathways and enhancement mechanisms within localized and non-localized transport regions in skin treated with low-frequency sonophoresis and sodium lauryl sulfate. J. Pharm. Sci. 100 (2), 512–529. https://doi.org/10.1002/jps.22280.

Polat, B.E., Hart, D., Langer, R., Blankschtein, D., 2011b. Ultrasound-mediated transdermal drug delivery: mechanisms, scope, and emerging trends. J. Control. Release 152 (3), 330–348. https://doi.org/10.1016/j.jconrel.2011.01.006.

Quiroz-Segoviano, R.I.Y., García-Sánchez, M.A., Delgado-Buenrostro, N.L., Chirino, Y.I., Bernal-Chávez, S., Nava-Arzaluz, M.G., Ganem-Rondero, A., 2019. Tetraphenylporphyrin intended for use in photodynamic therapy: influence of sonophoresis and the formulation (solution or microemulsion) on percutaneous penetration. J. Drug Deliv. Sci. Technol. 53, 1–10. https://doi.org/10.1016/j.jddst.2019.101145.

Schoellhammer, C.M., Polat, B.E., Mendenhall, J., Maa, R., Jones, B., Hart, D.P., Langer, R., Blankschtein, D., 2012. Rapid skin permeabilization by the simultaneous application of dual-frequency, high-intensity ultrasound. J. Control. Release 163 (2), 154–160. https://doi.org/10.1016/j.jconrel.2012.08.019.

Schoellhammer, C.M., Blankschtein, D., Langer, R., 2014. Skin permeabilization for transdermal drug delivery: recent advances and future prospects. Expert Opin. Drug Deliv. 11 (3), 393–407. https://doi.org/10.1517/17425247.2014.875528.

Scioli Montoto, S., Sbaraglini, M.L., Talevi, A., Couyoupetrou, M., Di Ianni, M., Pesce, G. O., Alvarez, V.A., Bruno-Blanch, L.E., Castro, G.R., Ruiz, M.E., Islan, G.A., 2018. Carbamazepine-loaded solid lipid nanoparticles and nanostructured lipid carriers: physicochemical characterization and in vitro/in vivo evaluation. Colloids Surf. B Biointerfaces 167, 73–81. https://doi.org/10.1016/j.colsurfb.2018.03.052.

Seto, J.E., Polat, B.E., Lopez, R.F.V., Blankschtein, D., Langer, R., 2010. Effects of ultrasound and sodium lauryl sulfate on the transdermal delivery of hydrophilic permeants: comparative in vitro studies with full-thickness and split-thickness pig and human skin. J. Control. Release 145 (1), 26–32. https://doi.org/10.1016/j.jconrel.2010.03.013.

Shah, P.P., Desai, P.R., Patel, A.R., Singh, M.S., 2012. Skin permeating nanogel for the cutaneous co-delivery of two anti-inflammatory drugs. Biomaterials 33 (5), 1607–1617. https://doi.org/10.1016/j.biomaterials.2011.11.011.

Shah, S., Rangaraj, N., Laxmikeshav, K., Sampathi, S., 2020. Nanogels as drug carriers – introduction, chemical aspects, release mechanisms and potential applications. Int. J. Pharm. 581, 1–16. https://doi.org/10.1016/j.ijpharm.2020.119268.

Shibaguchi, H., Tsuru, H., Kuroki, M., Kuroki, M., 2011. Sonodynamic cancer therapy: a non-invasive and repeatable approach using low-intensity ultrasound with a sonosensitizer. Anticancer Res 31 (7), 2425–2429. PMID: 21873154.

Shivam, U.U., Siddhi, K.C., Devarshi, U.G., Umeshkumar, M.U., Jayvadan, K.P., 2020. Nanoparticles laden In situ gel for sustained drug release after topical ocular administration. J. Drug Deliv. Sci. Technol. 57, 1–17. https://doi.org/10.1016/j.jddst.2020.101736.

Shokri, J., Nokhodchi, A., Dashbolaghi, A., Hassan-Zadeh, D., Ghafourian, T., Barzegar Jalali, M., 2001. The effect of surfactants on the skin penetration of diazepam. Int. J. Pharm. 228 (1–2), 99–107. https://doi.org/10.1016/s0378-5173(01)00805-5.

Silva, A.C., Amaral, M.H., González-Mira, E., Santos, D., Ferreira, D., 2012. Solid lipid nanoparticles (SLN)–based hydrogels as potential carriers for oral transmucosal delivery of risperidone: preparation and characterization studies. Colloids Surf. B Biointerfaces 93, 241–248. https://doi.org/10.1016/j.colsurfb.2012.01.014.

Sledge, W.G., Neuberg, D., Bernardo, P., Ingle, J.N., Martino, S., Rowinsky, E.K., Wood, W.C., 2003. Phase III trial of doxorubicin, paclitaxel, and the combination of doxorubicin and paclitaxel as front-line chemotherapy for metastatic breast cancer: an intergroup trial (E1193). J. Clin. Oncol. 21 (4), 588–592. https://doi.org/10.1200/JCO.2003.08.013.

Souto, E.B., Wissing, S.A., Barbosa, C.M., Müller, R.H., 2004. Evaluation of the physical stability of SLN and NLC before and after incorporation into hydrogel formulations. Eur. J. Pharm. Biopharm. 58 (1), 83–90. https://doi.org/10.1016/j.ejpb.2004.02.015.

Souza, C., de Freitas, L.A.P., Maia Campos, P.M.B.G., 2017. Topical formulation containing beeswax-based nanoparticles improved in vivo skin barrier function. AAPS PharmSciTech 18 (7), 2505–2516. https://doi.org/10.1208/s12249-017-0737-x.

Tang, H., Blankschtein, D., Langer, R., 2002. Effects of low-frequency ultrasound on the transdermal permeation of mannitol: comparative studies with in vivo and in vitro skin. J. Pharm. Sci. 91 (8), 1776–1794. https://doi.org/10.1002/jps.10164.

Tang, H., Mitragotri, S., Blankschtein, D., Langer, R., 2001. Theoretical description of transdermal transport of hydrophilic permeants: application to low-frequency sonophoresis. J. Pharm. Sci. 90 (5), 545–568. https://doi.org/10.1002/1520-6017(200105)90:5<545::AID-JPS1012>3.0.CO;2-H.

Taveira, S.F., Nomizo, A., Lopez, R.F.V., 2009. Effect of the iontophoresis of a chitosan gel on doxorubicin skin penetration and cytotoxicity. J. Control. Release 134 (1), 35–40. https://doi.org/10.1016/j.jconrel.2008.11.002.

Taveira, S.F., De Campos Araújo, L.M.P., De Santana, D.C.A.S., Nomizo, A., De Freitas, L. A.P., Lopez, R.F.V., 2012. Development of cationic solid lipid nanoparticles with factorial design-based studies for topical administration of doxorubicin. J. Biomed. Nanotechnol. 8 92), 219–228. https://doi.org/10.1166/jbn.2012.1383.

Taveira, S.F., De Santana, D.C., Araújo, L.M., Marquele-Oliveira, F., Nomizo, A., Lopez, R.F.V., 2014. Effect of iontophoresis on topical delivery of doxorubicin-loaded solid lipid nanoparticles. J. Biomed. Nanotechnol. 10 (7), 1382–1390. https://doi.org/10.1166/jbn.2014.1834.

Tezel, A., Sens, A., Tuchscherer, J., Mitragotri, S., 2002. Synergistic effect of low-frequency ultrasound and surfactants on skin permeability. J. Pharm. Sci. 91 (1), 91–100. https://doi.org/10.1002/jps.10000.

Tupal, A., Sabzichi, M., Ramezani, F., Kouhsoltani, M., Hamishehkar, H., 2016. Dermal delivery of doxorubicin-loaded solid lipid nanoparticles for the treatment of skin cancer. J. Microencapsul. 33 (4), 372–380. https://doi.org/10.1080/02652048.2016.1200150.

Wang, W., Zhang, P., Shan, W., Gao, J., Liang, W., 2013. A novel chitosan-based thermosensitive hydrogel containing doxorubicin liposomes for topical cancer therapy. J. Biomater. Sci. Polym. 24 (14), 1649–1659. https://doi.org/10.1080/09205063.2013.789357.

Wolloch, L., Kost, J., 2010. The importance of microjet vs shock wave formation in sonophoresis. J. Control. Release 148 (2), 204–211. https://doi.org/10.1016/j.jconrel.2010.07.106.

Zolochevska, O., Xia, X., Williams, B.J., Ramsay, A., Li, S., Figueiredo, M.L., 2011. Sonoporation delivery of interleukin-27 gene therapy efficiently reduces prostate tumor cell growth in vivo. Hum. Gene Ther. 22 (12), 1537–1550. https://doi.org/10.1089/hum.2011.076.